Real-time Rendering of porous surfaces and its applications

K. Hnat, D. Porquet, S. Merillou, D. Ghazanfarpour

MSI Laboratory LIMOGES France

Abstract

Matter reflection properties are a crucial factor in achieving a high degree of realism in image synthesis. The most common invisible defect having visible effects is roughness, handled by the majority of Bi-directional Reflectance Distribution Functions (BRDFs). However, porosity is also of great visual importance and is often omitted. It is a very common feature of real surfaces as it affects a variety of different materials (ceramics, building materials). Moreover, porosity is at the origin of a large number of weathering effects. These phenomena are of great importance in image synthesis as well as in other fields such as architecture or cultural heritage conservation. We propose in this paper to implement the porous surfaces BRDF postprocess model in real-time and to extend it to account for numerous weathering phenomena.

Key words: real-time rendering, porosity, reflection properties, weathering, polluted surfaces.

1 Introduction

The real-time rendering field produces more and more realistic images. To increase realism, light/matter interactions must be improved. As a first component of these interactions, valid light models have been proposed in the past years ([1][2]). An other fundamental component driving reflection properties is surface micro-geometry.
Human-visible geometric object features can be handled by geometrical techniques ([3]) or fake-geometrical techniques ([4]). Nevertheless, real surfaces exhibit some non human-visible micro-geometric features having global human-visible effects. Among these features, roughness has been taken into account in the great majority of Bi-directional Reflectance Distribution Functions (BRDFs). Porosity is another micro-geometric feature, often omitted in realistic rendering. However, it can modify significantly the optical properties of surfaces ([5]). The proportion of pores onto surfaces can be very important

(up to 0.4 in fired-clay bricks ([])).
Moreover, porosity is directly linked to numerous weathering processes. It is at the origin of destructive corrosion as it permits to chemical reactions to continue underneath the surface. Efflorescence is produced by wetting/drying cycles inside materials due to their porosity. Porosity can also explain changes in appearance of wet surfaces, becoming darker and more specular. It plays a key role in numerous other weathering processes such as painted or varnished surfaces tarnishing.
The 3D simulation of porous materials can be very important when dealing with cultural heritage conservation. Software permitting to simulate the behavior of buildings during their aging, may help to prevent some damages. Our approach is a first in step in conception of a realtime aging simulator, able to take into account a lot of natural phenomena. This paper deals with a real-time simulation of porous surfaces (based on a model presented in [6]). model [6], as well as extensions permitting to take into account some new natural phenomena, directly linked with porosity.
Related works are presented in section 2. Section 3 deals with the model itself. Then, each proposed extension is detailed in its own section (4.1, 4.2, 4.3). We also present obtained results in section 5. Finally, we conclude and present future works.

2 Related works

2.1 Local illumination models

Local illumination models importance has been early understood in image synthesis. Phong [7] has proposed a first model handling rough surfaces by providing a specular component controlled by an empiric roughness coefficient. To improve the physical validity of local illumination models, Cook and Torrance [8] have proposed a surface roughness model based on V-shapes and derived physical formulations from [9]. It allows to account for micro geometric-based behaviors (self-shadowing and masking effects) and to include Fresnel's laws. A generator based on a microfacet model can also be found in [10].
Physical description of surfaces has been further studied by He et al [11] improving, among other parameters, the surface roughness description using two characteristics instead of a single one: the RMS roughness and the autocorrelation length (mean distance between roughness peaks). A lot of other studies have been performed in the reflection modelling field, accounting for specific phenomena such as non-Lambertian diffuse reflection [12], anisotropic behaviors [13][14], diffraction [15] and layered materials [16]

Several authors have proposed other mathematical formulations of the previ-

ous models to improve their accuracy to real experiments [17], [18] or their computational efficiency [19]. Moreover, numerous non-analytical BRDF have been proposed (in [20] for example) but are beyond the scope of this paper. Furthermore, a recent state of art in reflectance modelling can be found in [21].
In the analytical models range, surface microgeometry description accounts only for roughness. To solve this problem, porosity has been introduced in [6] as a BRDF postprocess. This permits to provide this new microgeometric defect and to keep advantages provided by the postprocessed base BRDF.
When dealing with graphics hardware, the most used model are either the Phong or the Blinn-Phong model. These models are natively implemented into graphics pipeline. However, some works permits to use some others models (such as for instance [22]). As we use a BRDF postprocess [6], we can choose any analytical models to compute our images, in real time.

2.2 Weathering models

Weathering phenomena in computer graphics are of great importance because of their major visual influence. Due to the large amount of different physical processes and their complexity, numerous studies have focused on specific weathering phenomena. These techniques can be empirical or physically-based and can affect all the rendering pipeline (geometry, reflection properties, and colors).
Becket and Badler [23] have first handled surfaces imperfections by using a fractal based texture synthesis technique. Blinn [24] and Hsu [25] have proposed techniques to render surfaces covered by dust. Miller [26] has provided accessibility shading algorithms permitting to render tarnished surfaces. Wong has proposed a geometry dependent method in [27] to represent dust accumulation, patinas and peeling. In [28], authors modify objects geometry to handle impacts by different tools. Paint peeling and crackling have been investigated in [29].
In order to obtain more plausible results, some physically valid techniques have also been developed. Dorsey [30] proposed a model to take into account dirtiness brought onto surfaces by flow processes. Weathering of non-porous stones has been studied in [31]. Wet surfaces appearance has been studied in [32] . Corrosion (both patinas and destructive corrosion) has been investigated in [33] and [34]. A physically-based scratched surfaces model has been presented in [35].

In this paper, our approach is to provide a real-time generic model to take into account weathering processes directly linked with porosity.

3 The BRDF Post-Process

3.1 Description of the BRDF postprocess [6]

The model proposes to introduce a deformed cylindrical pore in the classical surface description used in local lighting computation. Pores distribution is supposed to be uniform over the surface. Their behavior is considered individually (light absorption and emission in the pore) and follows some principles:

- Incident light contribution to specular reflexion is replaced by a contribution to diffuse reflexion. This substitution is modulated by a masking and shadowing term (see below). Indeed, a pore can be shadowed by hills of surface.
- Contribution of incident lighting to diffuse reflection is modulated by total energy lost by light in the pore.

These phenomenological rules can be applied on any BRDF which can be separated into a diffuse and a specular component.
As described in [6], the model consist in introducing new specular and diffuse component called k_{s-poro} and k_{d-poro} which take into account porosity. The new model can be written as:

$$f_r = k_{d-pore}.F_s + k_{d-pore}.F_d \tag{1}$$

With:

$$k_{s-poro} = k_s.(1 - \alpha.G_p) \tag{2}$$

$$k_{d-poro} = k_d.(1 - \alpha.G_p.A_p) + k_s.\alpha.G_p.(1 - A_p) \tag{3}$$

- α is the fraction of surface covered with pores
- s_p is the fraction between the mean depth of the pores and their average diameter.
- G_p is the shadowing and masking terms used classically in the microfacets based BRDF models

$$G_p = \frac{(N.S)}{(N.S) - k.(N.S) + k}.\frac{(N.V)}{(N.V) - k.(N.V) + k},\ k = \frac{2.m^2}{\pi} \tag{4}$$

  with m, the surface RMS roughness.
- A_p represents the total light loss in the pore. With n_b (number of bounces in the pores) and k_a (the total fraction of absorbed light,$k_a = 1 - k_s - k_d$),

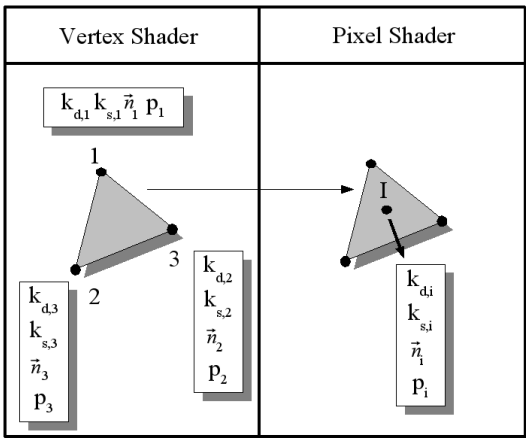

Fig. 1. Vertex and Pixel Shader network. Point 1,2,3 are triangle vertices. I is the interpolated point.

A_p may be written as:

$$A_p = k_a.\frac{1-(1-k_a)^{n_b}}{1-(1-k_a)} \tag{5}$$

$$n_b = s_p.[3.7 - 2.(\frac{\theta_i + \theta_r}{2} - \frac{2.\pi}{s_p + 6})] \tag{6}$$

3.2 Real-time rendering of porosity

Real time rendering of porosity was implemented using NVIDIA Cg and OpenGL. GPU's flexibility permits to directly implement per-pixel lighting without any approximation. As shown in the figure 1, the vertex shader computes k_s and k_d lighting parameters (i.e. Phong BRDF specular and diffuse components) at each triangle's vertices. This shader also gathers geometrical data (normal and position of each vertex), which are its variable parameters. However, for the shader itself, some other parameters are constant, such as light position or camera transformation matrix. These values do not depend on object vertices. During rasterization, vertex shader output data are interpolated over the triangle's surface. These data are used to compute color at a given pixel. The BRDF postprocess is fully implemented into a pixel shader. Using $k_{d,i}$ and $k_{s,i}$, the interpolated value of BRDF specular and diffuse components, we compute the $k_{d,poro}$ and $k_{s,poro}$ as defined in section 3.

4 Extension of porosity BRDF postprocess

Porosity of materials is of great importance when one deals with some natural phenomena. We choose to extend the porous model. We propose to use a phenomenological approach in order to take into account some of these phenomena. It permits to obtain physically plausible results and to keep model simple and intuitive

4.1 Atmospheric pollution of porous materials.

With the increase of atmospheric pollution due to combustion of different kind of fuel, many monument made with porous stones are attacked. Among such degradations, atmospheric pollution is considered as a major factor of change in visual aspect. The next section describes the alteration of porous surfaces by atmospheric pollution. Then, we present a model to account for this weathering alteration.

4.1.1 Atmospheric pollution phenomenon

The two previous centuries have seen a strong increase of energy production and consumption, due to transport and manufactures development. The use of new combustible (fuel, kind of fuels) have led to important sulphur emission in atmosphere (SO_4 under gaseous form and particles like soot). Consequently, sulfatation of cultural heritage materials is very common[36].
Atmospheric pollution effects on stones can be divided into three non-uniform areas, depending on pollution types, materials, geometry and rain exposition. When observing such polluted surface, one can found these areas: *white area*, *grey area* and *black area* as shown in figure 2.

4.1.1.1 Grey area. This area is protected from rain and water streaming. Particles deposition on the surface (atmospheric pollution) causes this change in color. This phenomenon depends on the material roughness: particles are blocked into grooves of surface microgeometry. A layer of gypsum ($CaSO_4$) grow up on the materials without affecting visible geometry [37] [38]. However, these particles are very sensitive to water flow down: any water streaming may stop the growing process. Phenomenologically, only object parts kept away from water are submitted to this phenomenon.

4.1.1.2 Black area. Blackening is due to a deposit of particles inside materials pore. These pores are filled with carbon particles issued from wood and

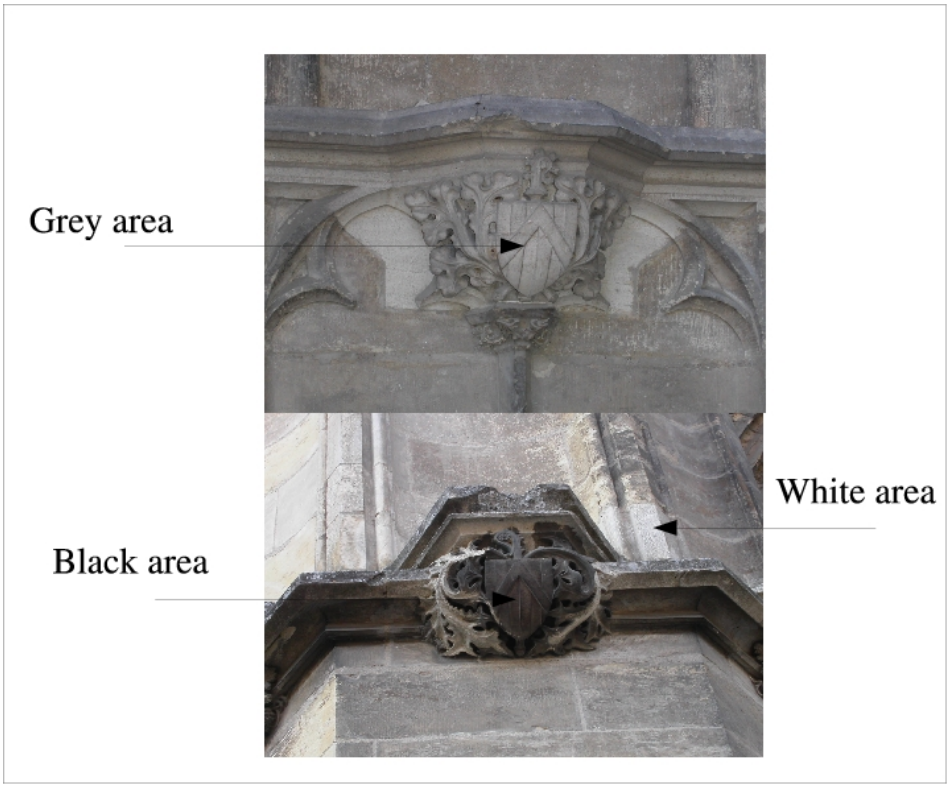

Fig. 2. Pollution area

petroleum combustion. This phenomenon always comes with gypsum ($CaSO_4$) formation which cement the particles inside the pore. Very porous stones (like sandstone) with a very important roughness factor are very sensitive to blackening. Therefore, particles are trapped into the pores and nothing can bring them up (even water rain or air) except chemical/mechanical cleaning, which is a costly operation, when possible. Intensity of this phenomenon depends on particles concentration in atmosphere and material characteristics. We can notice that a part of blackening can be due to development of organisms colored in black which preferred humidity to develop each other (like moss). Phenomenologically, this kind of pollution develops itself particularly in holes and salient edges.

4.1.1.3 White area. This area is the erosion area, submitted to rain and water streaming. Rain cleans up surfaces, bringing up the particles. In this area, objects keep their natural color. Particles deposited between two rain falls are evacuated by the next water streaming and the gypsum created is dissolved.

Based on the described phenomenological behavior, we propose a method to simulate real-time aging of porous stones.

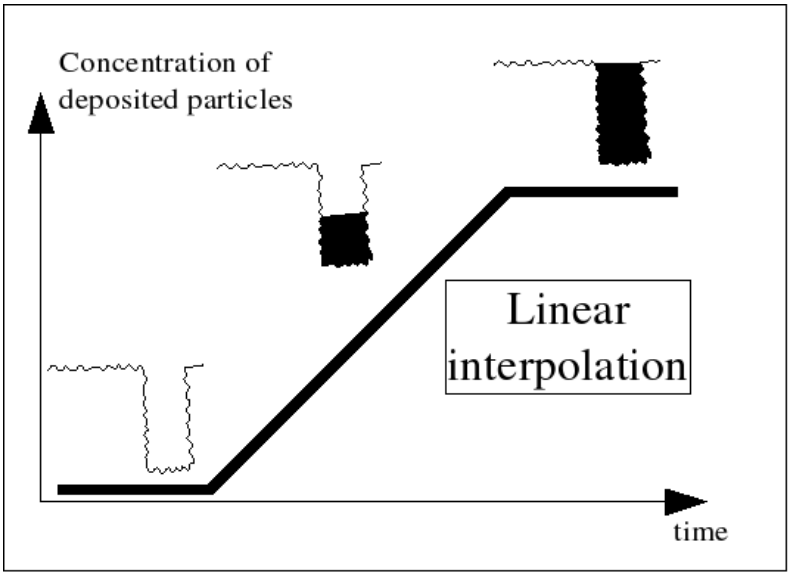

Fig. 3. Pore filling up over the time.

4.1.2 Description of the method

Our method is based on the phenomenological observations made in the previous section. The effect of weathering on the geometry itself is considered as negligible. Therefore, we only simulate aging phenomena using the BRDF postprocess [6]. First, we extend this porous postprocess to integrate soiling. Then, we explain how to detect the three parts of weathering described in the previous section.

4.1.2.1 Integrating dirtiness into porous-BRDF As previously described, the white area is characterized by rain cleaning up of materials. Consequently, the white area behaves like the original material. We will use the original porous BRDF postprocess to render such area.

The black area is due to a deposit of carbon particles in the pore. Gypsum cements the particles and no natural phenomenon can clean the surface. As shown in the figure 3, evolution of particles deposition may be decomposed in three parts:

- Particles deposition is slow. Pores start to be filled with particles. Nothing changes in material visual appearance.
- Particles deposition increases very quickly. Pores are filled with a great number of particles. Gypsum is created and cements the particles into the pores. The visual aspect of the affected material changes.
- Pores are entirely filled with carbon particles. The deposition of particles is stopped. The darkening is at maximum.

To describe this weathering effect, we use the BRDF postprocess described in the section 3. When porous materials are filled with particles, the porous component of postprocess is changed. As described in section 4.1.1, the particles are essentially composed of carbon. Consequently, they are black and have a diffuse behavior. In this case, only the diffuse part of the porous BRDF is changed. The specular and diffuse energy ratio reflected by pore itself is replaced by a diffuse part accounting for pollutant as shown in figure 4.

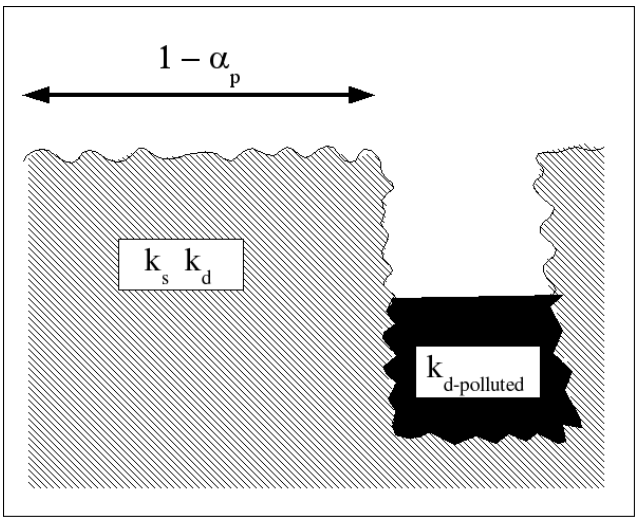

Fig. 4. Pore partially filled with pollutant.

$$k_{d-poro-polluted} = k_d.(1 - \alpha.G_p) + k_{d-pollution}.\alpha.G_p.(1 - A_p) \quad (7)$$

$k_{d-pollution}$ is the diffuse coefficient of the deposited particles and can be choose near of 0.8. As described in the section 4.1.2.1, pores geometry change (height reduced). Consequently, number of bounces into the pores decreased. To simulate this behavior, we introduce a linear interpolation of geometrical term s_p between initial value of s_p (i.e intrinsic material value) and 0 (pore wholly filled with material). This change implies a modification of A_p, the total loss in the pore.

4.1.2.2 Conception of the texture representing the white area The white area as defined in section 4.1.1 describes the part of a mesh submitted to rain. As we study porous materials, we approximate that the water streaming is negligible. Therefore, a object parts receives water directly comes from the sky. We must estimate the preferential area which receives water. We simulate this process using a light map. Surface area light is sized to represent all the possible incident directions of rain fall as shown in figure 6(a). We obtain a 2D light map as shown in figure 6(b). The texture will also give us informations about the grey area. Indeed, a fully masked point will be in a grey area (The grey area in the complementary of the white area).

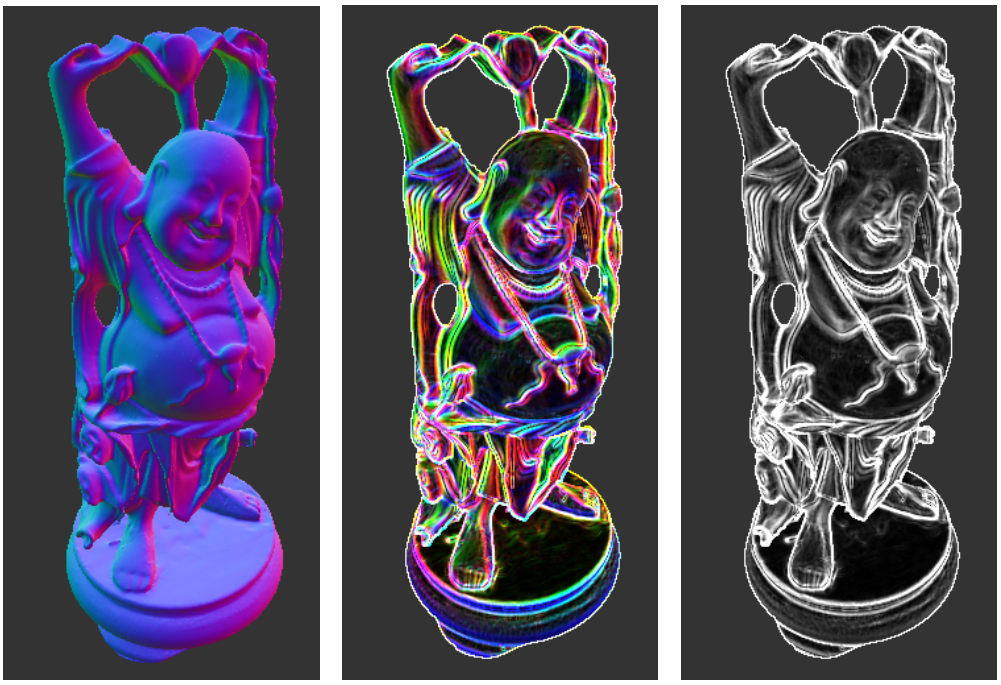

(a) normal map (b) Sobel filter (c) Average Sobel filter

Fig. 5. Normal map and Sobel filter on a Buddha

(a) scene used to obtain lightmap (b) buddha lightmap

Fig. 6. Light map principle and example

4.1.2.3 Real-time Rendering. As described in the section 4.1, the black area begins to grow in the holes and on the edges. We must consider a method to detect these particular parts of an object. For this purpose, we use the normals map of the object (as shown in the figure 5(a)). This map is filtered

-1	-2	-1
0	0	0
+1	+2	+1

-1	0	+1
-2	0	+2
-1	0	+1

Table 1
Sobel horizontal and vertical convolution matrix

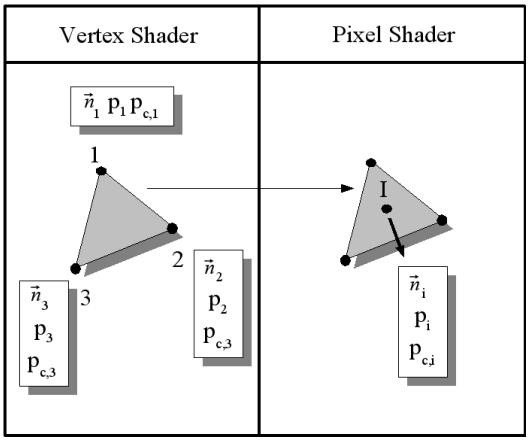

Fig. 7. Vertex and Pixel Shader network before Sobel filtering. Point 1,2,3 are triangle vertices. I is the interpolated point. p_c is a projective coordinate used to compute the Sobel filtering.

using a simple Sobel edge detector. This filter emphasizes the preferential area of pollution deposition, giving for each pixel, the amount of variation of normal onto the surface (i.e. hollow and bump areas). Figure 5(a) exhibits the filtered normal map mapped onto the original mesh. A hard edge color will be white on the Sobel map. This color is used as a threshold making soiling to progressively appear on the object.

Sobel filtering is done using capability of GPU. Indeed, to compute the normal map, we use a pixel shader which outpout a color corresponding to the interpolated normal at considered point. With $\overrightarrow{n}(n_x, n_y, n_z)$, the output color is simply $C_{RGB} = (\frac{n_x+1}{2}, \frac{n_y+1}{2}, \frac{n_z+1}{2})$. To filter this normal map, we render into a texture called T_n the mesh mapped with the normal map. As this rendering is not put into the framebuffer, this operation is very fast (see [39]). Then, we display the mesh and apply the Sobel edge detector. For each pixel $p_i(x, y)$ of T_n, we apply horizontal S_h and vertical S_v Sobel detector. The Sobel filter depends on projective coordinate (x, y) interpolated into the pixel shader as shown in figure 7. Using these coordinates, we apply the Sobel convolution matrix (recalled at table 1) on the texture T_n. The figure 5(b) display a Buddha with $|S_h| + |S_v|$. Average of this value ($\overline{|S_h| + |S_v|}$) gives a gray level texture as shown in figure 5(c).

4.2 Wet and porous surfaces

4.2.1 Wetting surface process

Porous surfaces may be wet by rain falls or by other interactions. Wet surfaces have already been studied by Jensen et al in [32] . In this paper, authors introduced the change in materials behavior because of wetting, making materials darker, brighter, more specular or translucent. The model is based on a two layer surface reflection model. In this section, we propose to simulate the same behavior in the case of porous surfaces.

This phenomenon is quite simple. Water falls onto a porous surface. Porous are filled with water. This observation is based on real measurement of water penetration into porous surfaces studied in material science.

4.2.2 Wet porous surface model

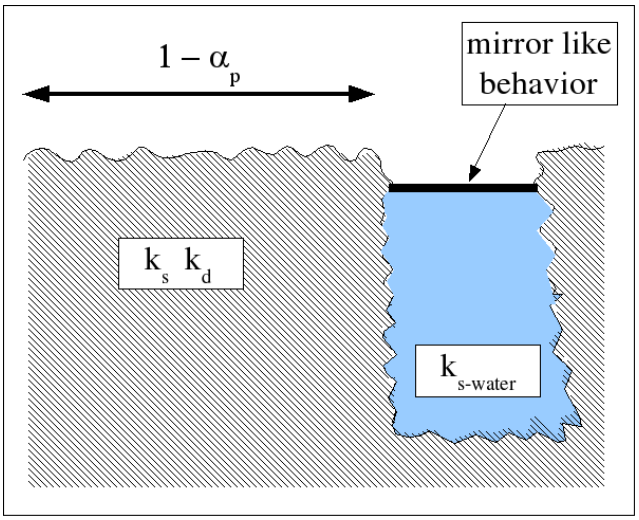

Fig. 8. Pore partially filled with water.

The figure 8 exhibits part of a porous surface. Non porous part of the surface is considered as not wet. We consider the pore progressively filled with water. In this case, we can approximate the behavior of such surface like a only specular surface (near of mirror-like behavior). Pore contribution to diffuse reflexion is replaces by a contribution to specular reflection due to water.

$$k_{s-wet} = k_s(1 - \alpha.G_p) + k_{s-water}.\alpha.G_p(1 - A_p) \quad (8)$$

$$k_{d-wet} = k_d.(1 - \alpha.G_p) \quad (9)$$

$k_{s-water}$ is the water specular coefficient (value near of 1). To increase the realism of rendering, we use the light map used to estimate received rain in

section 4.1.2.2. We obtain the objects parts submitted to rain falls. Surfaces always submitted to water will be in white. On the other hand, surfaces which are never wet are in black. To simulate the evolution wetting with time, we use a threshold with this map. Surfaces with high weight in the lightmap will be wet first. When we decrease our threshold, the wet surface increases. The same real time implementation as described in section 4.1 can be used. The pixel shader is changed to take into account for the new formula of k_{s-wet} and k_{d-wet}.

4.3 Image based real-time rendering of efflorescence

4.3.1 Efflorescence formation process

Efflorescence is a thin layer of salt deposited inside pores surfaces [40]. The appearance of efflorescence implies an aesthetic and an economic problem. Efflorescence may appear on brick, block masonry and leads to a color change of human constructions. Consequently, cleaning and restoring such construction is a strong economic problem. Moreover, formation of an important efflorescence layer may imply some structural damages and can endanger the construction in some cases.

Many parameters control efflorescence formation. For instance, it depends on environmental circumstance, material parameters or chemical composition. Water charged with salts penetrates in materials. Migration of water from heart to material surface using inner capillary structure leads to salt deposition. The main origin of efflorescence is the brick/mortar interaction, where migrations occurs with high salts concentration (due to mortar). During drying/wetting cycle, pores are filled with salts with a diffuse component material. Chemical composition of efflorescence gives its color (mostly white but eventually green or brown) [41]. Moreover, it is easily observable that efflorescence salts is a diffuse matter. Efflorescence was first introduces in computer graphics in [42] using 3D texture.

4.3.2 Integrating efflorescence into porous model.

As previously done, we use the porous model and integrate a simple phenomenological description of efflorescence formation. The figure 9 exhibits the model basis.

$$k_{s-poro-efflo} = k_s.(1 - \alpha.G_p) \tag{10}$$

$$k_{d-poro-efflo} = k_d.(1 - \alpha.G_p.A_p) + k_{d-efflo}.\alpha.G_p.(1 - A_p) \tag{11}$$

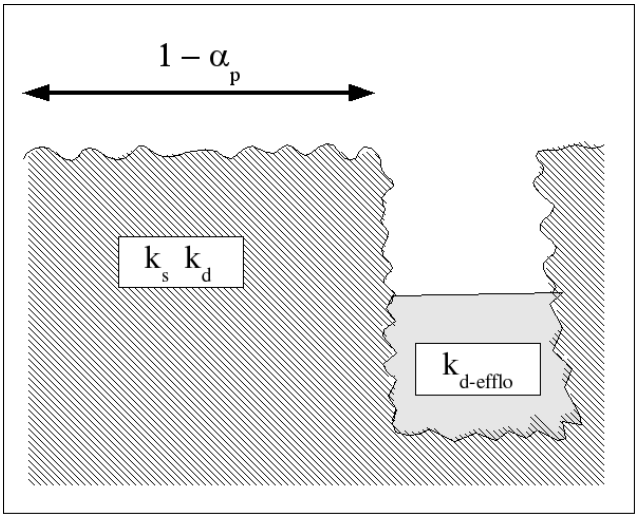

Fig. 9. Pore partially filled with salt crystal.

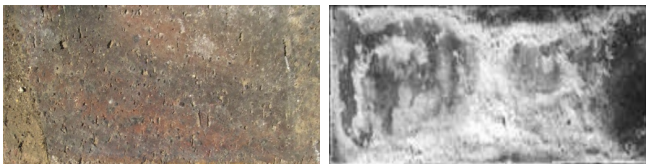

Fig. 10. Texture used in efflorescence rendering

$k_{d-efflo}$ is the diffuse coefficient of efflorescence constituent (near of 0.8).

Furthermore, to increase realism, position of efflorescence on the brick is very important. As previously stated, efflorescence develops itself preferentially at the interface mortar/brick. As this localization is very complex (it depends on numerous phenomena), we propose to use a real photography of brick to synthesize an efflorescence location texture. This image based technique reinforce the realism of efflorescence rendering. We convert a real efflorescence photography into height field map. While the pore is wholly filled, it emit a only diffuse color (generally white). To take into account salt crystal, we decrease linearly s_p to take into account the geometry change.

In our approach, one texture is used to control the localization and the evolution of the efflorescence on the brick. The second texture gives the material color. Texture are shown in figure 10. The shader used these textures to compute color of each pixel. We modify the BRDF postprocess to interate the phenomenon described in section 4.3.1

5 Results

Figure 11 shows a comparaison between Phong lighting model and our BRDF porous model (based on the same Phong parameters). Figure 12 exhibits the progressive soiling of a Caryatid model. Figure 14 and 13 respectively shows the wetporous surfaces and the efflorescence. Videos and pictures gathering all this results can be downloaded at http://msi.unilim.fr/∽porquet/simpra/index.html. We used NVIDIA CG compiler [43] and OpenGL [39] to implement our method using NVIDIA GeForceFX 6800GT. All texture resolutions were set to 512×512 pixels. The frame rate mainly depends on underlying hardware, nevertheless we obtain high frame rate. For instance, the Caryatide model composed of 100k triangles is rendered at 200FPS . The complexity of our shaders are presented in table 2.

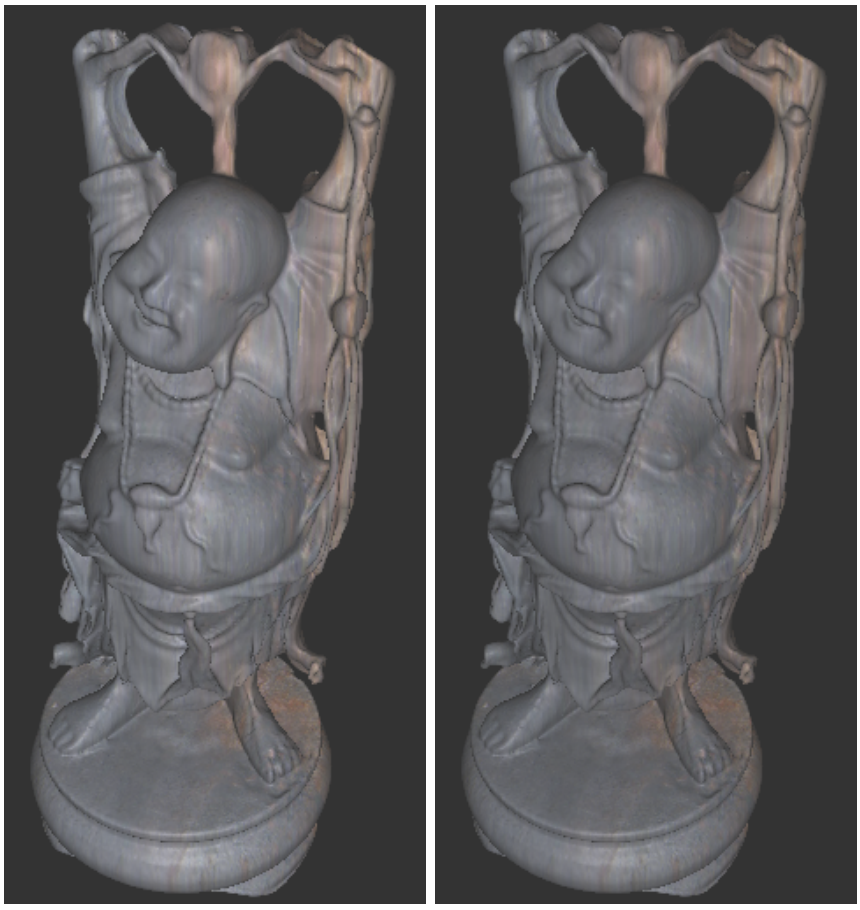

(a) Phong (b) Phong and porosity

Fig. 11. Real-time BRDF postprocess

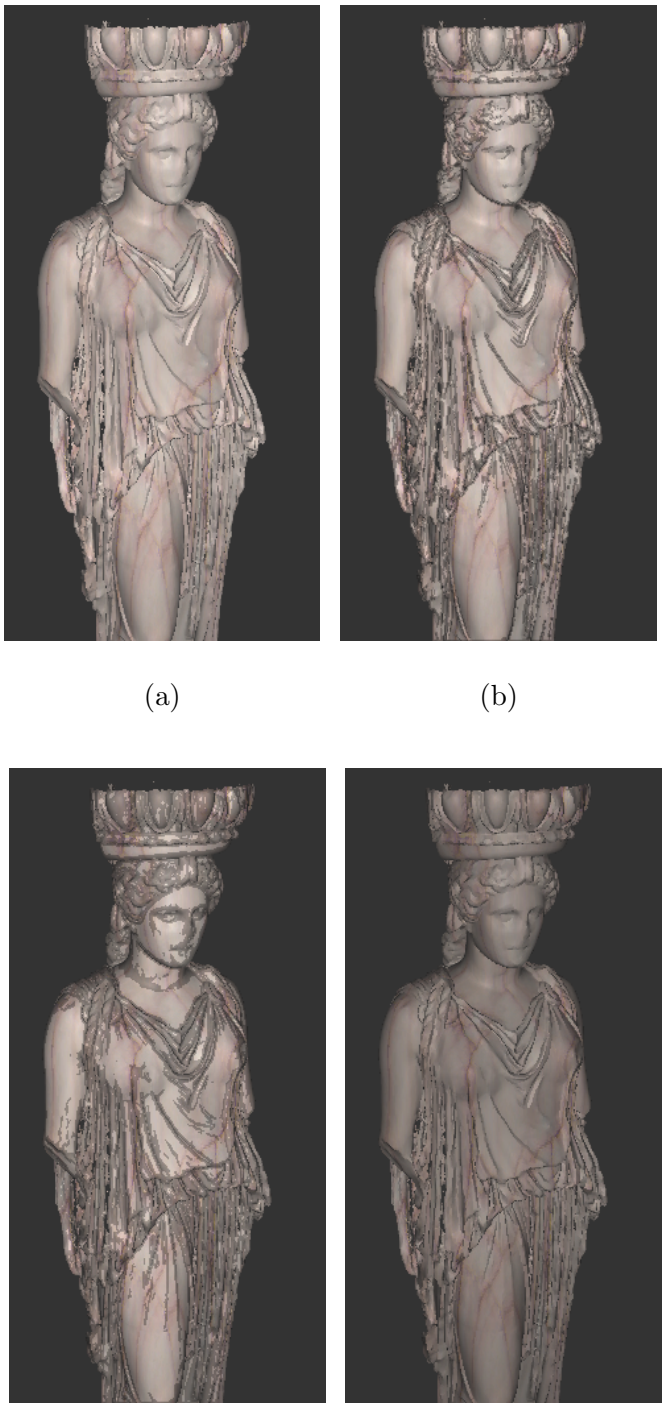

(a) (b)

(c) (d)

Fig. 12. Soiling effect on the Caryatid

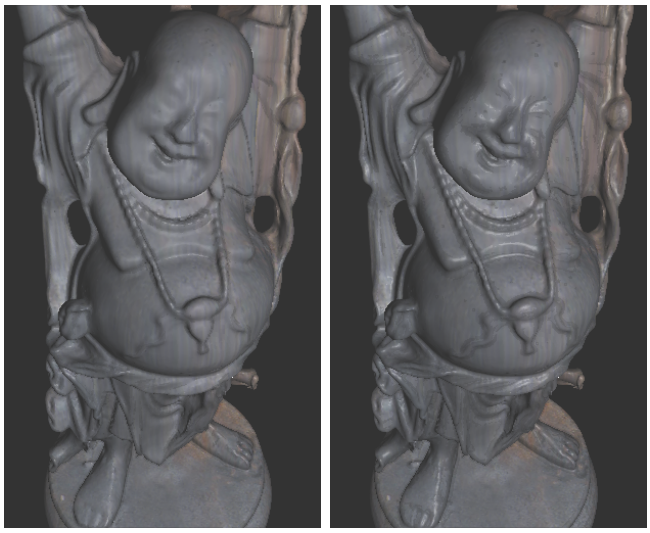

Fig. 13. Wet and porous surfaces

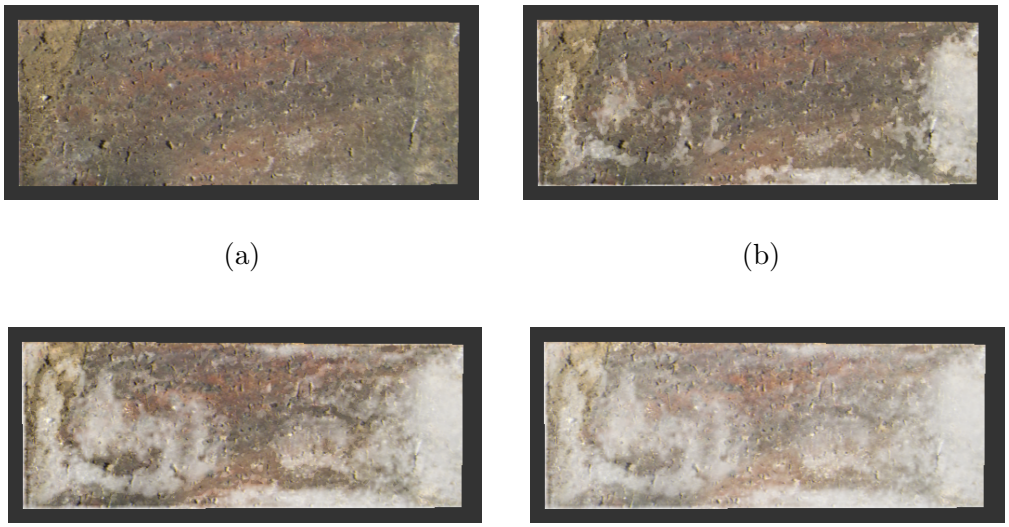

(a) (b)

(c) (d)

Fig. 14. Efflorescence Results

	Porosity	Soiling	Wet surfaces	Efflorescence
♯ instructions	83	138	120	101
♯ texture fetch	1	8	7	2

Table 2
Pixel shaders characteristic of our real-time implementation

6 Conclusion and future works

In this paper we have introduced porous surface rendering in real-time. Our technique permits to account for such surfaces on a realistic manner. Moreover, porosity is the main origin of a lot of different weathering processes and changes in appearance. We have introduced extensions to the porosity model, permitting to render specific weathering processes in real-time. Beyond their visual importance, these defects can be useful in several other fields such as architecture or cultural heritage preservation as our tool permits to detect weathered zones for example. Moreover, a phenomenological approach is simple and intuitive.

On one hand, as future works, we aim to introduce new weathering phenomena linked with porosity. For example, appearance evolution due to varnish applied on porous surfaces such as wood, or paint penetration underneath surfaces are greatly influenced by this parameter. We can also improve our current efflorescence model to predict the position onto bricks
On other hand, porosity alone is not sufficient to accurately handle these appearances as one have to use multi-layer reflection properties and more specifically light interactions between these layers. Furthermore, it seems important for the realistic image synthesis field to provide real physically-based weathering models, to increase results accuracy.

7 Acknowledgment

Maya Software has been used with agreements of ALIAS© to compute the light map. 3D models are courtesy of Paul Debevec and Stanford university.

References

[1] A. S. Glassner, Principles of Digital Image Synthesis, Morgan Kaufmann Publishers Inc., 1994.

[2] P. Shirley, R. K. Morley, Realistic Ray Tracing, A. K. Peters, Ltd., 2003.

[3] R. L. Cook, Shade trees, in: Proceedings of the 11th annual conference on Computer graphics and interactive techniques, ACM Press, 1984, pp. 223–231.

[4] J. F. Blinn, Simulation of wrinkled surfaces, in: Proceedings of the 5th annual conference on Computer graphics and interactive techniques, ACM Press, 1978, pp. 286–292.

[5] C. J. Brinker, G. W. Scherer, Sol-gel science, academic press, inc. Edition, Harcourt Brace and Company Publishers, SanDiego, 1990.

[6] S. Merillou, J.-M. Dischler, D. Ghazanfarpour, A brdf post-process to integrate porosity on rendered surfaces, in: IEEE Transaction on Vizualisation and Computer Graphics, Vol. 6, 2000, pp. 306–318.

[7] B. T. Phong, Illumination for computer generated pictures, in: Commun. ACM, Vol. 18, ACM Press, 1975, pp. 311–317.

[8] R. L. Cook, K. E. Torrance, A reflectance model for computer graphics, in: Proceedings of the 8th annual conference on Computer graphics and interactive techniques, ACM Press, 1981, pp. 307–316.

[9] K. E. Torrance, E. Sparrow, Theory for off-specular reflection from roughned surfaces, in: Journal of the optical society of America, Vol. 57, 1967.

[10] M. Ashikhmin, S. Premoze, P. Shirley, A microfacet-based brdf generator, in: SIGGRAPH '00: Proceedings of the 27th annual conference on Computer graphics and interactive techniques, ACM Press/Addison-Wesley Publishing Co., New York, NY, USA, 2000, pp. 65–74.

[11] X. D. He, K. E. Torrance, F. X. Sillion, D. P. Greenberg, A comprehensive physical model for light reflection, in: Proceedings of the 18th annual conference on Computer graphics and interactive techniques, ACM Press, 1991, pp. 175–186.

[12] M. Oren, S. K. Nayar, Generalization of lambert's reflectance model, in: SIGGRAPH '94: Proceedings of the 21st annual conference on Computer graphics and interactive techniques, ACM Press, 1994, pp. 239–246.

[13] P. Poulin, A. Fournier, A model for anisotropic reflection, in: Proceedings of the 17th annual conference on Computer graphics and interactive techniques, ACM Press, 1990, pp. 273–282.

[14] M. Ashikhmin, P. Shirley, An anisotropic phong light reflection model, in: Journal of graphics tools, 2000.

[15] J. Stam, Diffraction shader, in: A. Glassner (Ed.), Proc. SIGGRAPH '99. ACM SIGGRAPH, ACM Press, 1999, pp. 75 – 84.

[16] X. Granier, W. Heidrich, A simple layered rgb brdf model, in: Graph. Models, Vol. 65, Academic Press Professional, Inc., San Diego, CA, USA, 2003, pp. 171–184.

[17] G. J. Ward, Measuring and modeling anisotropic reflection, in: Proceedings of the 19th annual conference on Computer graphics and interactive techniques, ACM Press, 1992, pp. 265–272.

[18] E. P. F. Lafortune, S.-C. Foo, K. E. Torrance, D. P. Greenberg, Non-linear approximation of reflectance functions, in: SIGGRAPH '97: Proceedings of the 24th annual conference on Computer graphics and interactive techniques, ACM Press/Addison-Wesley Publishing Co., New York, NY, USA, 1997, pp. 117–126.

[19] C. Schlick, An inexpensive BRDF model for physically-based rendering, in: Computer Graphics Forum, Vol. 13, 1994, pp. 233–246.

[20] S. H. Westin, J. R. Arvo, K. E. Torrance, Predicting reflectance functions from complex surfaces, in: Proceedings of the 19th annual conference on Computer graphics and interactive techniques, ACM Press, 1992, pp. 255–264.

[21] M. Ashikhmin, P. Shirley, S. Marschner, J. Stam, State of the art in modeling and measuring of surface reflection, in: SIGGRAPH Courses 2001, 2001.

[22] J. Kautz, H.-P. Seidel, Hardware accelerated displacement mapping for image based rendering, in: GRIN'01: No description on Graphics interface 2001, Canadian Information Processing Society, 2001, pp. 61–70.

[23] W. Becket, N. Badler, Imperfection for realistic image synthesis, in: Journal of Visualization and Computer Animation, Vol. 1, 1990, pp. 26 – 32.

[24] J. F. Blinn, Light reflection functions for simulation of clouds and dusty surfaces, in: Computer Graphics, Vol. 16, 1982, pp. 21 – 29.

[25] S. Hsu, T. Wong, Simulating dust accumulation, in: IEEE Computer Graphics and Applications, Vol. 15, 1995, pp. 18 – 22.

[26] G. Miller, Efficient algorithms for local and global accessibility shading, in: ACM SIGGRAPH, 1994, pp. 319 – 326.

[27] T. T. Wong, W. Y. Ng, P. A. Heng, A geometry dependent texture generation framework for simulating surface imperfections, in: Proceedings of Eurographics Workshop on Rendering, 1997, pp. 139 – 150.

[28] E. Paquette, P. Poulin, G. Drettakis, Surface aging by impacts, in: Graphics Interface, 2001, pp. 175 – 182.

[29] E. Paquette, P. Poulin, G. Drettakis, The simulation of paint cracking and peeling, in: Graphics Interface, 2002, pp. 59 – 68.

[30] J. Dorsey, H. Pedersen, P. Hanrahan, Flow and changes in appearance, in: ACM SIGGRAPH, 1996, pp. 411 – 420.

[31] J. Dorsey, A. Edelman, H. Jensen, J. Legakis, H. Pedersen, Modeling and rendering of weathered stone, in: ACM SIGGRAPH, 1999, pp. 225 – 234.

[32] H. W. Jensen, J. Legakis, J. Dorsey, Rendering of wet materials, in: E. D. Lischinski, G. W. Larson (Eds.), Rendering Techniques '99, springer-verlag Edition, 1999, pp. 273 – 282.

[33] J. Dorsey, P. Hanrahan, Modeling and rendering of metallic patinas, in: ACM SIGGRAPH, 1996, pp. 387 – 396.

[34] S. Merillou, J.-M. Dischler, D. Ghazanfarpour, Corrosion: Simulating and rendering, in: Graphics Interface, 2001, pp. 167 – 174.

[35] C. Bosch, S. Merillou, X. Pueyo, D. Ghazanfarpour, A physically-based model for rendering realistic scratches, in: Computer Graphics Forum, Vol. 23, Eurographics 2004, pp. 361–370.

[36] R. V. Grieken, F. Delalieux, K. Gysels, Cultural heritage and the environment, in: Pure and Applied Chemistry, Vol. 70, p. p. 2327.

[37] P. Ausset, F. Bannery, M. D. Monte, R.-A. Lefèvre, Recording of pre-industrial atmospheric environment by ancient crusts on stone monuments, in: Atmospheric Environment, Vol. 32, 1998, pp. 2859 – 2863.

[38] A. Baulig, J. J. Poirault, P. Ausset, R. Schins, T. Shi, D. Baralle, P. Dorlhene, M. Meyer, R. Lefèvre, A. Baeza-Squiban, F. Marano, Physicochemical characteristics and biological activities of seasonal atmospheric particulate matter sampling in two locations of paris, in: Environmental Science and Technology, Vol. 22, 2004, pp. 5985 – 5992.

[39] Opengl architectural review board arb_fragment program opengl extension, in: http://oss.sgi.com/projects/oglsample/registry/ARB/fragment_program.txt.

[40] L. Hennetier, J. V. Almeida, A. M. S. Correira, V. M. Ferreira, Efflorescence and its quantification in ceramic building materials, in: Br. Ceram. Trans., Vol. 100, 2001, pp. 72 – 76.

[41] H. Brocken, T. G. Nijland, White efflorescence on brick masonry and concrete masonry blocks, with special emphasis on sulfate efflorescence on concrete blocks, in: Construction and Building Materials, Vol. 18, 2004, pp. 315 – 323.

[42] S. S.Shahidi, D. Ghazanfarpour, Phenomenological simulation of efflorescence in brick constructions, in: MSI Technical Report submitted to publication, no. 2005-02.

[43] Nvidia corporation http://developer.nvidia.com.